Axisymmetric radiation intensity model for annular reactors

Baoqing Deng*, Kaiyang Ye, and Bensheng Zhao

Department of Environmental Science and Engineering, University of Shanghai for Science and Technology, Shanghai 200093, P R China

Short title: Axisymmetric radiation intensity model

Abstract

Cylindrical lamps are usually equipped in the tubular UV reactor to offer UV radiation. This paper describes the axisymmetric characteristics of UV radiation from the cylindrical UV lamp. Axisymmetric lamp emission models are developed in a two-dimensional axisymmetric space for the line source, the superficial source and the volumetric source. The present axisymmetric lamp emission models are easy to understand and of simple mathematical expressions. The experimental data in literature is used to validate the present axisymmetric lamp emission models. Good agreements have been obtained between the experimental data and the computations. A comparison show that the present models obtain the identical results as previous models.

Keywords: annular reactor; radiation distribution; Axisymmetric radiation

*corresponding author: bqdeng@usst.edu.cn

Highlights:

1. Axisymmetric characteristics of radiation from the cylindrical UV lamp is presented.

2. Axisymmetric lamp emission models are developed.

3. The present models obtain the same result as the previous models.

1 INTRODUCTION

UV reactors have been widely used in disinfection and photocatalysis. In disinfection, UV light destroys the DNA of microorganisms. In photocatalysis, the electron-hole pair is excited on the surface of photocatalyst under the illumination of UV light and involved in the oxidation of organic pollutants. In short, UV light plays an important role in UV reactors. UV light is usually generated by UV lamps installed either outside the reactor or inside the reactor. Thus, correct simulation of lamp emission is a must to obtain the radiation intensity inside the reactor.

The simplest lamp emission model views the lamp as some discrete points emitting photons along the axis of lamp.[1,2] The accuracy may depend on the number of discrete point sources. In order to avoid choosing the number of discrete point sources, line source models were developed. Depending on the manner of photon emission, line source models are categorized into line source spherical emission model (LSSE) and line source diffuse emission model (LSDE). The photons are assumed to be emitted in a spherical manner in the LSSE[3,4] and in a diffuse manner in the LSDE,[3] respectively. In nature, line source emission models are the variant of point source model with infinite points. Line source emission models have gained popularity because of their simple mathematical expressions,[5–9] however, which may bring about error when the reactor dimension is not large with respect to the UV lamp.[10]

Many efforts have been made to improve the accuracy of line source emission models by viewing the lamp as a superficial source or a volumetric source. For the superficial source model, the lamp is modelled as a cylindrical surface, from which photons are emitted into the space in a spherical manner or in a diffuse manner. A spherical emission leads to an extensive source spherical emission (ESSE) model[11] whereas a diffuse emission leads to an extensive source diffuse emission (ESDE) model.[12] Different mathematical expressions of ESSE and ESDE were also presented in literature, namely SSSE and SSDE model.[13–15] For the volumetric source model, the lamp is modeled as a cylinder and the emitters distributes uniformly inside the cylinder. By fixing the coordinate origin at the observed point, extense volumetric source emission models (EVSE) were developed.[16–21] The EVSE has been proved to precisely simulate the radiation field.[22–24] However, the EVSE was thought to have the highest complexity.[25] By fixing the coor-

dinate origin at the lamp, a volume source emission (VSE) model was developed.[14,15,26]

The above-mentioned lamp emission models have been validated and widely used in the simulation of radiation intensity in UV reactors.[6,27–33] A common feature of the above-mentioned models is that they only considered the energy emitted from the UV lamp onto a single observed point. To the best of authors' knowledge, the relation of energies received by different points has never been studied. In the present study, the axisymmetric lamp emission models are developed. Good agreements are obtained between the present axisymmetric lamp emission models and the experimental data as well as the previous lamp emission models.

2 Model development

2.1 Axisymmetry of lamp emission

In the derivation of previous lamp emission models, there existed three kinds of assumptions on the lamp geometry, the radiation emission and the reactor: (1) The lamp was a cylinder. The lamp can be simplified as a line, a cylindrical surface or a perfect cylinder, respectively; (2) The emitters were distributed within the source and each emitter had the same radiation characteristics; (3) The reactor was cylindrical and filled with a transparent fluid. No absorption, scattering and reflection in the reactor was considered. Based on these assumptions, the above-mentioned lamp emission models were developed.

An important feature that was not paid attention previously is the axisymmetry of a cylindrical lamp in geometry, as shown in Figure 1. It has been widely assumed that the emitters inside the lamp are uniform and homogeneous.[16–21] Thus, the lamp emission must be axisymmetric also. The circle in Figure 1 is perpendicular to the axis of UV lamp and its center is at the axis of UV lamp. Thus, for any points located at this circle such as A and B, the fluence rate received on the points must be the same. When the lamp is simplified as a line, a cylindrical surface or a prefect cylinder, this axisymmetry always exists, which can be used to simplify lamp emission models.

Consider a control volume in the cylindrical coordinate encompassed by surfaces S1, S2 and S3, as shown in Figure 2. The z axis is the symmetric axis of UV lamp. r_0 is the radius of lamp. The surface S1 is a piece of sphere with the point O $(r = 0, z = h)$ as its

center and occupies from $\varphi = 0$ to $\varphi = \pi$. Surfaces S2 and S3 are two azimuthal planes in the cylindrical coordinate. The control volume ($\theta \sim \theta + d\theta, h - \frac{1}{2}dh \sim h + \frac{1}{2}dh, 0 \sim r_0$) represents the true UV lamp element at $z = h$. For the line source model and the superficial source model, the lamp emission element is modelled as a line element ($h - \frac{1}{2}dh \sim h + \frac{1}{2}dh, r = 0$) and a surface element ($\theta \sim \theta + d\theta, h - \frac{1}{2}dh \sim h + \frac{1}{2}dh, r = r_0$), respectively. Following the energy conservation law, we have

$$\frac{K_L}{2\pi} d\theta dh = E_{1,L} + E_2 + E_3 \tag{1}$$

for the line source, or

$$K_A r_0 d\theta dh = E_{1,A} + E_2 + E_3 \tag{2}$$

for the superficial source, or

$$K_V d\theta dh \int_0^{r_0} RdR \ = E_{1,V} + E_2 + E_3 \tag{3}$$

for the volumetric source. K_L, K_A and K_V are the energy emitted per unit length of lamp, per unit surface area of lamp and per unit volume of lamp, respectively. The left-hand side of Eqs. (1)-(3) represents the total energy emitted from the emitter inside the control volume in Figure 2. The terms of right-hand side of Eqs. (1)-(3) are the energy passing surfaces S1, S2 and S3, respectively. The axisymmetry of the emission from the cylindrical lamp must yield

$$E_2 = E_3 = 0 \tag{4}$$

Thus, we can obtain

$$\frac{K_L}{2\pi} d\theta dh = E_{1,L} \tag{5}$$

for the line source, or

$$K_A r_0 d\theta dh = E_{1,A} \tag{6}$$

for the superficial source, or

$$K_V d\theta dh \int_0^{r_0} RdR = E_{1,V} \tag{7}$$

for the volumetric source.

Eqs. (5)-(7) describes the energy incident onto the surface S1 for different assumptions of lamp, which will be used to derive the fluence rate in the reactor.

2.2 Axisymmetric lamp emission models

Line source emission

The area of surface S1 can be calculated as

$$dA = 2\left[r^2 + (z-h)^2\right] d\theta \tag{8}$$

In case of the spherical emission, the fluence rate at the point P on the surface S1 due to the emission of line element $(h - \frac{1}{2}dh \sim h + \frac{1}{2}dh, r = 0)$ can be evaluated by

$$dG\left(\vec{r}\right) = \frac{E_{1,L}}{dA} \tag{9}$$

where G is the fluence rate at the point P ($\mathrm{W\,m^{-2}}$. By using Eq. (5), we can obtain

$$dG\left(\vec{r}\right) = \frac{K_L dh}{4\pi\left[r^2 + (z-h)^2\right]} \tag{10}$$

The integration to Eq. (10) along the lamp yields[2,4,5]

$$\begin{aligned} G\left(\vec{r}\right) &= \int_{-L}^{L} \frac{K_L r dh}{4\pi\left[r^2 + (z-h)^2\right]} \\ &= \frac{K_L}{4\pi r}\left[\arctan\left(\frac{z+L}{r}\right) - \arctan\left(\frac{z-L}{r}\right)\right] \end{aligned} \tag{11}$$

In case of the diffuse emission, the fluence rate at the point P emitted from the line element $(h - \frac{1}{2}dh \sim h + \frac{1}{2}dh, r = 0)$ can be evaluated by

$$dG\left(\vec{r}\right) = \frac{K_L r dh}{\pi^2\left[r^2 + (z-h)^2\right]^{1.5}} \tag{12}$$

Numerical integration to Eq. (12) was performed to obtain the fluence rate.[4,15] As a matter of fact, the integration to Eq. (12) along the lamp can yield an analytical

expression as follows

$$\begin{aligned} G\left(\vec{r}\right) &= \int_{-L}^{L} \frac{K_L r dh}{\pi^2 \left[r^2 + (z-h)^2\right]^{1.5}} \\ &= \frac{K_L}{\pi^2 r}\left(\frac{z+L}{\sqrt{r^2+(z+L)^2}} - \frac{z-L}{\sqrt{r^2+(z-L)^2}}\right) \end{aligned} \tag{13}$$

Eqs. (11) and (13) are identical to the LSSE and LSDE in literature. Note that there doesn't exist the azimuthal coordinate, meaning an axisymmetric feature.

2.3 Superficial source emission

When the UV lamp is modelled as a superficial source, all radiation is emitted from a cylindrical surface, i.e., the outside surface of UV lamp. Since the surface element($\theta \sim \theta + d\theta, h - \frac{1}{2}dh \sim h + \frac{1}{2}dh, r = r_0$) can be viewed as a differential plane, only the region of $\varphi \in (\alpha \sim \pi - \alpha)$ on the surface S1 can receive the radiation, where the angle α can be calculated from

$$\cos\alpha = \frac{\left[r^2 + (z-h)^2 - r_0^2\right]^{0.5}}{\left[r^2 + (z-h)^2\right]^{0.5}} \tag{14}$$

The effective area on the surface S1 that can receive the radiation is

$$dA_{eff} = 2\cos\alpha \left[r^2 + (z-h)^2\right] d\theta \tag{15}$$

Assuming that the energy emitted from the surface element distributes uniformly on the effective area of the surface S1, the fluence rate at the point P due to the emission of the surface element can be evaluated by

$$dG\left(\vec{r}\right) = \frac{E_{1,A}}{dA_{eff}} \tag{16}$$

By using Eq. (6), we can obtain

$$dG\left(\vec{r}\right) = \frac{K_A r_0 dh}{2\left[r^2 + (z-h)^2\right]^{0.5}\left[r^2 + (z-h)^2 - r_0^2\right]^{0.5}} \tag{17}$$

The integration to Eq. (17) along the lamp yields

$$G\left(\vec{r}\right)=\int_{-L}^{L}\frac{K_A r_0 dh}{2\left[r^2+\left(z-h\right)^2\right]^{0.5}\left[r^2+\left(z-h\right)^2-r_0^2\right]^{0.5}} \tag{18}$$

Herein, Eq. (18) is the axisymmetric superficial source emission model, namely A-SSE model. Compared with previous superficial model, the present model doesn't require the integration with respect to azimuthal coordinate.

2.4 Volumetric source emission

Volumetric source models simulate the lamp as a cylinder and the emitters distribute uniformly inside the cylinder. In the control volume shown in Figure 2, $(\theta \sim \theta + d\theta, h-\frac{1}{2}dh \sim h+\frac{1}{2}dh, 0 \sim r_0)$ is the actual volumetric source, which can be viewed as an assembly of superficial sources $(\theta \sim \theta + d\theta, h-\frac{1}{2}dh \sim h+\frac{1}{2}dh, r=R \in (0 \sim r_0))$. Following Eq. (17) , the fluence rate at the point P due to the emission of $(\theta \sim \theta + d\theta, h-\frac{1}{2}dh \sim h+\frac{1}{2}dh, r=R)$ can be written as

$$dG\left(\vec{r}\right)=\frac{K_V R d\theta dh dR}{2d\theta\left[r^2+\left(z-h\right)^2\right]^{0.5}\left[r^2+\left(z-h\right)^2-R^2\right]^{0.5}} \tag{19}$$

or

$$dG\left(\vec{r}\right)=\frac{K_V R dh dR}{2\left[r^2+\left(z-h\right)^2\right]^{0.5}\left[r^2+\left(z-h\right)^2-R^2\right]^{0.5}} \tag{20}$$

The integration to Eq. (20 along the lamp yields

$$\begin{aligned} G\left(\vec{r}\right) &= \int_{-L}^{L}\int_{0}^{r_0}\frac{K_V R dh dR}{2\left[r^2+\left(z-h\right)^2\right]^{0.5}\left[r^2+\left(z-h\right)^2-R^2\right]^{0.5}} \\ &= K_V L-\frac{K_V}{2}\int_{-L}^{L}\left[1-\frac{r_0^2}{r^2+\left(z-h\right)^2}\right]^{0.5}dh \end{aligned} \tag{21}$$

Herein, Eq. (21 is the axisymmetric volumetric source emission model, namely A-VSE model. Compared with previous volumetric models, only teh integration with respect to one coordinate is required in the present model.

3 RESULTS AND DISCUSSION

3.1 Validation with the experimental data

Three experiments are used to validate the present model. Jacob and Dranoff [1] measured the radiation profiles for different media in an annular reactor. The diameter of UV lamp is 0.63 inch. The effective lamp length is 4 inch. The experimental data were presented using a relative fluence rate. Rahn et al. [34] conducted the measurement of fluence rate distribution in UV reactors. The length of lamp is 150 mm. The diameter of lamp is 10 mm. The output power of lamp was estimated to be 3.84 W. Li et al. [35] measured fluence rate in UV reactors using a micro fluorescent silica detector. The length of UV lamp is 297 mm. The diameter of UV lamp is 16 mm. The output power is estimated as 4.48 W. The latter two experiments gave the experimental data of fluence rate.

Figure 3 shows the relative fluence rates computed from A-SSE and A-VSE models. The experimental data are found to be slightly greater than the computed values, which was also proven for the LSSE model by Jacob and Dranoff [1] and for the LSDE model and the EVSE model by Irazoqui et al. [16]. In general, good agreements between the present models and the experimental data are obtained.

Figure 4 displays the comparison of the present model and the experiment. Both the A-SSE model and the A-VSE coincide with each other. A relative error of model values within 20-25% of the experimental data was thought to be acceptable.[34] However, the computed fluence rate for the output power given by Rahn et al. [34], 3.84 W, is 25% greater than the experimental data for a small radial distance. This error can be ascribed to the overestimated output power. Rahn et al. [34] assumed that the irradiance was uniform on a sphere with a radius of 1 m around the lamp centroid. The irradiance was measured at a distance of 1 m from the lamp along the axis perpendicular to the center of the lamp. Then the output power was estimated by multiplying this value with the area of sphere. However, it was reported that the irradiance had a cosine-like feature.[30] The irradiance measured by Rahn et al. [34] is the largest among all irradiance values. Thus, the estimated output power may be greater than the actual value. It was proved that the output power may be overestimated around 20%.[36] Thus, the output power is modified as 3.07 W. As shown in Figure 4, the profile with the modified power is close to the experimental data with a maximum error 25% at the first point.

Figure 5 shows the distribution of fluence rate along the radial distance. The present model overestimated the fluence rate compared with the experimental data. Model overestimation was also observed and ascribed to the cylindrical shape of micro fluorescent silica detector.[33] By introducing the angular response correction, Ahmed et al. [33] obtained the computational result in accordance with the experimental data. However, the estimation of output power of Li et al. [35] is the same as that of Rahn et al. [34]. That is, the output power may be overestimated. A modified output power is 3.6 W. As shown in Figure 5, the modified profile is in good agreement with the experimental data. Li et al. [35] measured the fluence rate along the reactor height at four radius positions. With the modified output power, the fluence rate along the reactor height is calculated using the present models. As shown in Figure 6, Good agreements between the present models and the experimental data are obtained. The maximum error is 13% observed, however, which doesn't exceed the range recommended by Rahn et al. [34].

3.2 Comparison with other models

When UV lamps are viewed as a superficial source or a volumetric source, the present A-SSE and A-VSE models are different from previous models in mathematical expression. Herein the same configuration as [1] [1] will be used to compare the present models and the SSSE model and the VSE model.

Figure 7 shows fluence rate profiles computed using the A-SSE model and the SSSE model at two radial positions and two heights, respectively. The height $z = 0$ cm and $z = 5$ cm mean the center of lamp and the end of lamp, respectively. The maximum fluence rate at $z = 0$ cm is greater than that at $z = 5$ cm. However, both profiles decay fast along the radial direction, as shown in Figure 7a. The profile of $r = 0.8$ cm, close to the surface of the lamp, concentrates between $z = -5$ cm and $z = 5$ cm. With the increase of radius, fluence rate becomes flat along the height. In each figure, the profiles computed from two models coincide with each other at the same position. That is, both the present A-SSE model and the SSSE model obtain the nearly identical computational result.

Figures 8 shows fluence rate profiles using the present A-VSE model and the VSE model at two radial positions and two heights, respectively. The same tendency as Figure 7 can be observed in Figure 8. However, the maximum values computed by the

volumetric model are less than those computed by the superficial model because the emitter source in the superficial model is more close to the observed point than the volumetric source model. On the other hand, when the radial coordinate is relatively big, both the superficial source model and the volumetric source model obtain the nearly identical result, such as profiles for $r = 5\,\text{cm}$ shown in Figure 7b and Figure 8b.

4 Conclusions

The present paper describes the axis-symmetry of lamp emission in annular reactors. Axisymmetric lamp emission models are derived for superficial and volumetric sources, which has a simple mathematical expression.

The present axisymmetric lamp emission models are validated against the experiment on fluence rate in literature. Good agreements have been obtained between the present model and the experimental data on relative fluence rate in an annular reactor.

The present axisymmetric lamp emission models are also validated for fluence rate measured using spherical detector and cylindrical detector. Both experiments have been reproduced by using a corrected lamp output power.

A compression between the present axisymmetric lamp emission models and SSSE and VSE models are conducted. All models have obtained nearly identical results.

References

1. Jacob, S. M. and Dranoff, J. S. Light intensity profiles in a perfectly mixed photoreactor. *AIChE Journal* 1970;16 (3):359–363.

2. Bolton, J. R. Calculation of ultraviolet fluence rate distributions in an annular reactor: significance of refraction and reflection. *Water Research* 2000;34 (13):3315–3324.

3. Akehata, T. and Shirai, T. Effect of light-source characteristics on the performance of circular annular photochemical reactor. *J. Chem. Eng. Jpn* 1972;5 (4):385–391.

4. Blatchley, E. R. Numerical modelling of UV intensity: application to collimated-beam reactors and continuous-flow systems. *Water Research* 1997;31 (9):2205–2218.

5. Pareek, V. K. and Adesina, A. A. Light intensity distribution in a photocatalytic reactor using finite volume. *AIChE Journal* 2004;50 (6):1273–1288.

6. Yang, Q., Pehkonen, S. O., and Ray, M. B. Performance Evaluation of Light Emission Models in Light Attenuating Media. *Ozone: Science & Engineering* 2005;27 (6):459–467.

7. Salvadó-Estivill, I., Brucato, A., and Li Puma, G. Two-Dimensional Modeling of a Flat-Plate Photocatalytic Reactor for Oxidation of Indoor Air Pollutants. *Industrial & Engineering Chemistry Research* 2007;46 (23):7489–7496.

8. Salvadó-Estivill, I., Hargreaves, D. M., and Li Puma, G. Evaluation of the Intrinsic Photocatalytic Oxidation Kinetics of Indoor Air Pollutants. *Environmental Science & Technology* 2007;41 (6):2028–2035.

9. Qi, N., Zhang, H., Jin, B., and Zhang, K. CFD modelling of hydrodynamics and degradation kinetics in an annular slurry photocatalytic reactor for wastewater treatment. *Chemical Engineering Journal* 2011;172 (1):84–95.

10. Romero, R. L., Alfano, O. M., Marchetti, J. L., and Cassano, A. E. Modelling and parametric sensitivity of an annular photoreactor with complex kinetics. *Chemical Engineering Science* 1983;38 (9):1593–1605.

11. Stramigioli, C., Santarelli, F., and Foraboschi, F. P. Photosensitized reactions in an annular continuous photoreactor. *Applied Scientific Research* 1977;33 (1):23–44.

12. Yokota, T., Iwano, T., and Tadaki T. Light intensity in an annular photochemical reactor. *Kagaku Kogaku Ronbunshu* 1976;2 (3):298–303.

13. Pareek, V. K., Chong, S., Tadé, M., and Adesina, A. A. Light intensity distribution in heterogeneous photocatalytic reactors. *Asia-Pacific J. Chemical Engineering* 2008;3 (2):171–201.

14. Boyjoo, Y., Ang, M., and Pareek, V. Some aspects of photocatalytic reactor modeling using computational fluid dynamics. *Chemical Engineering Science* 2013;101:764–784.

15. Boyjoo, Y., Ang, M., and Pareek, V. Lamp emission and quartz sleeve modelling in slurry photocatalytic reactors. *Chemical Engineering Science* 2014;111:34–40.

16. Irazoqui, H. A., CerdÎó, J., and Cassano, A. E. Radiation profiles in an empty annular photoreactor with a source of finite spatial dimensions. *AIChE Journal* 1973;19 (3):460–467.

17. Irazoqui, H. A., Cerdá, J., and Cassano, A. E. The radiation field for the point and line source approximations and the three-dimensional source models: Applications to photoreactions. *The Chemical Engineering Journal* 1976;11 (1):27–37.

18. Alfano, O. M., Romero, R. L., and Cassano, A. E. Radiation field modelling in photoreactors—I. homogeneous media. *Chemical Engineering Science* 1986;41 (3):421–444.

19. Alfano, O. M., Vicente, M., Esplugas, S., and Cassano, A. E. Radiation field inside a tubular multilamp reactor for water and wastewater treatment. *Industrial & Engineering Chemistry Research* 1990;29 (7):1270–1278.

20. Romero, R. L., Alfano, O. M., and Cassano, A. E. Cylindrical Photocatalytic Reactors. Radiation Absorption and Scattering Effects Produced by Suspended Fine Particles in an Annular Space. *Industrial & Engineering Chemistry Research* 1997;36 (8):3094–3109.

21. Martínez Retamar, M. E., Passalía, C., Brandi, R. J., and Labas, M. D. Dose estimation methodology for the UV inactivation of bioaerosols in a Continuous-Flow reactor. *Aerosol Science and Technology* 2019;53 (1):8–20.

22. Vicente, M., Alfano, O. M., Esplugas, S., and Cassano, A. E. Design and experimental verification of a tubular multilamp reactor for water and wastewater treatment. *Industrial & Engineering Chemistry Research* 1990;29 (7):1278–1283.

23. Tymoschuk, A. R., Alfano, O. M., and Cassano, A. E. The multitubular photoreactor. 1. Radiation field for constant absorption reactors. *Industrial & Engineering Chemistry Research* 1993;32 (7):1328–1341.

24. Labas, M. D., Brandi, R. J., Zalazar, C. S., and Cassano, A. E. Water disinfection with UVC radiation and H_2O_2. A comparative study. *Photochemical & photobiological sciences* 2009;8 (5):670–676.

25. Coenen, T., van de Moortel, W., Logist, F., Luyten, J., van Impe, J. F., and Degrève, J. Modeling and geometry optimization of photochemical reactors: Single-

and multi-lamp reactors for UV–H2O2 AOP systems. *Chemical Engineering Science* 2013;96:174–189.

26. Boyjoo, Y., Sun, H., Liu, J., Pareek, V. K., and Wang, S. A review on photocatalysis for air treatment: From catalyst development to reactor design. *Chemical Engineering Journal* 2017;310:537–559.

27. Yang, Q., Pehkonen, S. O., and Ray, M. B. Evaluation of three different lamp emission models using novel application of potassium ferrioxalate actinometry. *Industrial & Engineering Chemistry Research* 2004;43 (4):948–955.

28. Yang, Q., Pehkonen, S. O., and Ray, M. B. Light Distribution Model for an Annular Reactor with a Cylindrical Reflector. *Industrial & Engineering Chemistry Research* 2005;44 (10):3471–3479.

29. Palmer, P. Fullana-i, Puig-Vidal, R., Celma, P. J., and Vilaseca, J. Photochemical reactors design: Light emission models description for anular reactors. Part 1, Classic models. *AFINIDAD* 2009;66 (541):206–213.

30. Duran, J. E., Taghipour, F., and Mohseni, M. Irradiance modeling in annular photoreactors using the finite-volume method. *Journal of Photochemistry and Photobiology A: Chemistry* 2010;215:81–89.

31. Elyasi, S. and Taghipour, F. General method of simulating radiation fields using measured boundary values. *Chemical Engineering Science* 2010;65 (20):5573–5581.

32. Palmer, P. Fullana-i, Puig-Vidal, R., Sanjosé, D., and Celma, P. Photoreactors design: Light emission models description for annular reactors. Part 2: Extense source models. *AFINIDAD* 2014;66 (542):278–284.

33. Ahmed, Y. M., Jongewaard, M., Li, M., and Blatchley, E. R. Ray Tracing for Fluence Rate Simulations in Ultraviolet Photoreactors. *Environmental Science & Technology* 2018;52 (8):4738–4745.

34. Rahn, R. O., Bolton, J., and Stefan, M. I. The Iodide/Iodate Actinometer in UV Disinfection: Determination of the Fluence Rate Distribution in UV Reactors. *Photochemistry and Photobiology* 2006;82 (2):611–615.

35. Li, M., Qiang, Z., Li, T., Bolton, J. R., and Liu, C. In situ measurement of UV fluence rate distribution by use of a micro fluorescent silica detector. *Environmental science & technology* 2011;45 (7):3034–3039.

36. Whitby, G. E., Sotirakos, B., and Bolton, J. R. A comparison of two methods for measuring the UV output of low pressure mercury lamps in air. *Proceedings of the Water Environment Federation* 2008;2008 (13):3877–3889.

5 Figure Captions

Figure 1 Schematic of axisymmetry for a cylindrical lamp

Figure 2 Schematic of control volume in a cylindrical coordinate

Figure 3 Fluence rate profiles at the mid-depth of the reactor and $z = -2$ inch

Figure 4 Fluence rate along radial direction

Figure 5 Fluence rate along radial direction at lamp center

Figure 6 Fluence rate along axial direction at four radial positions

Figure 7 Fluence rate profiles computed using the A-SSE model and the SSSE model. (a) at two heights (b) at two radial positions.

Figure 8 Fluence rate profiles computed using the A-VSE model and the VSE model. (a) at two heights (b) at two radial positions.

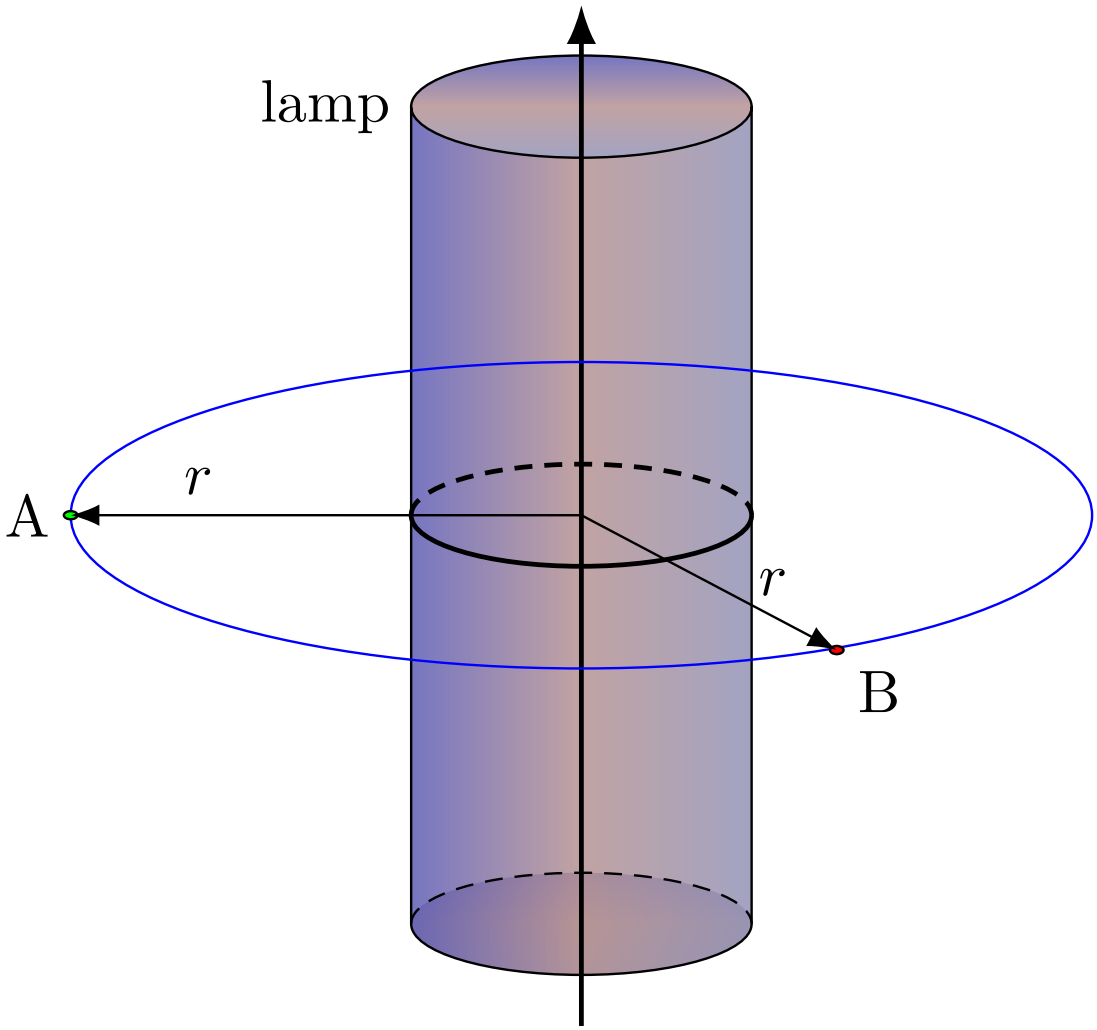

Figure 1

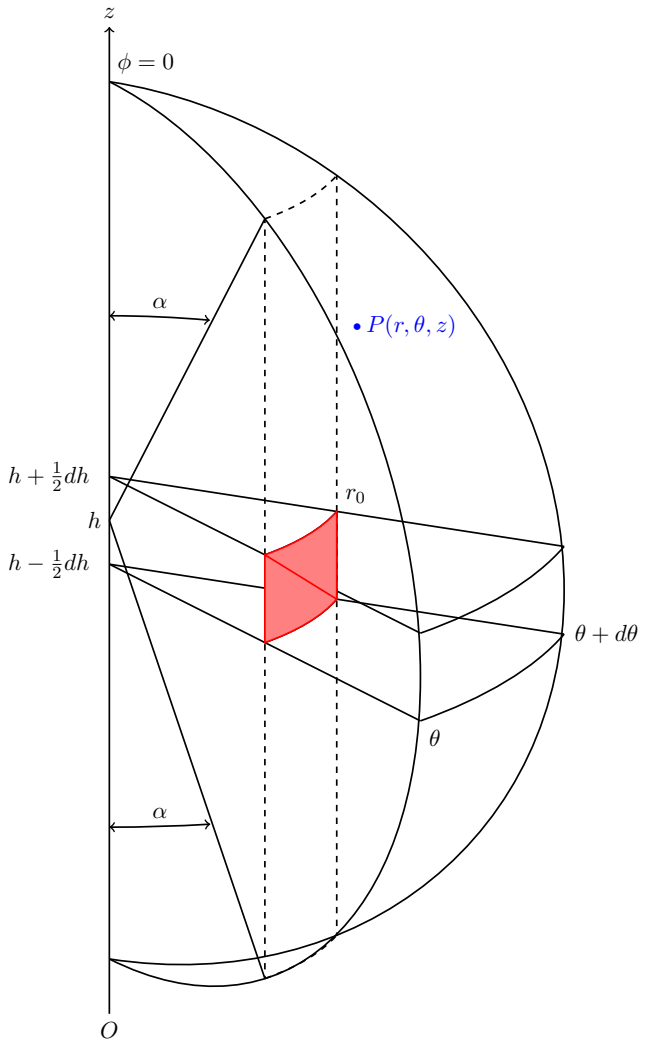
z
$\phi = 0$
α
$P(r, \theta, z)$
$h + \frac{1}{2}dh$
r_0
h
$h - \frac{1}{2}dh$
$\theta + d\theta$
θ
α
O

Figure 2

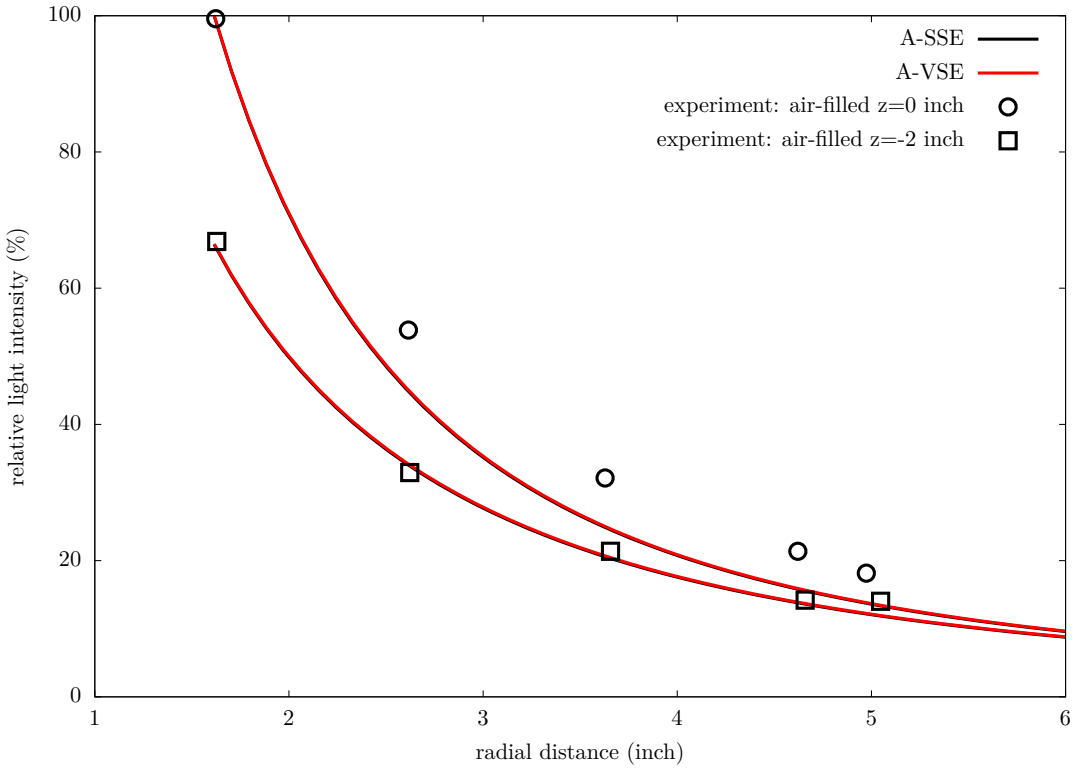
A-SSE
A-VSE
experiment: air-filled z=0 inch
experiment: air-filled z=-2 inch
relative light intensity (%)
radial distance (inch)
0
20
40
60
80
100
1
2
3
4
5
6

Figure 3

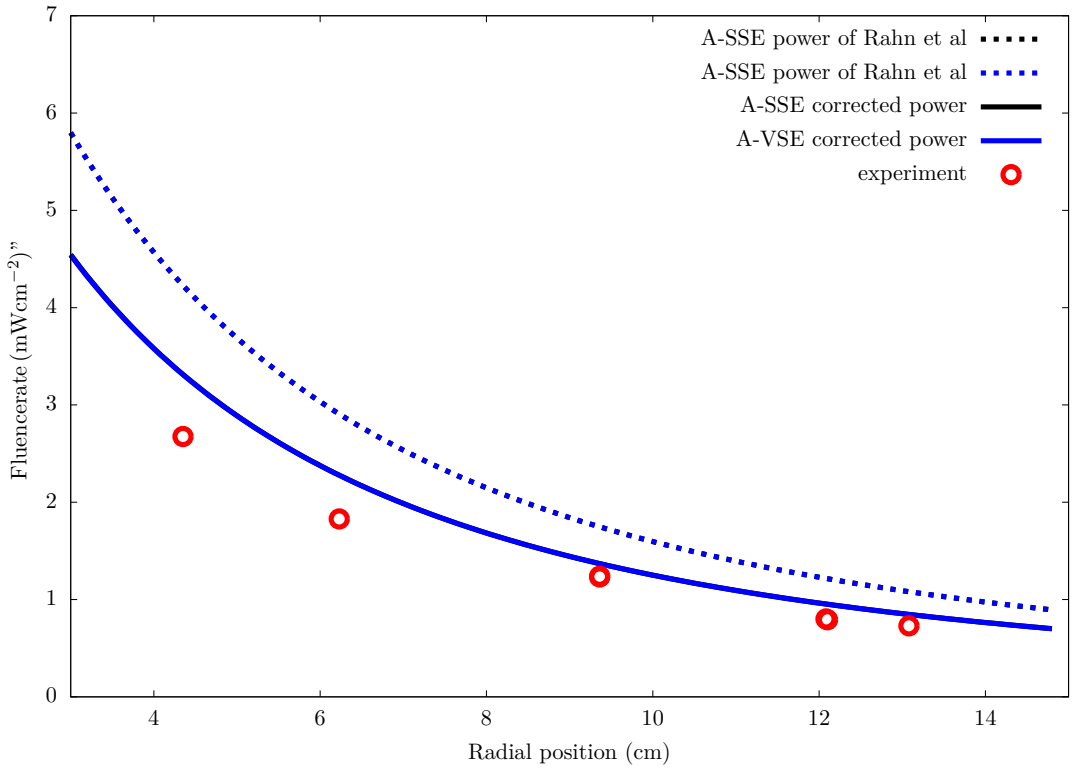
A-SSE power of Rahn et al
A-SSE power of Rahn et al
A-SSE corrected power
A-VSE corrected power
experiment
Fluencerate (mWcm^{-2})"
Radial position (cm)
0
1
2
3
4
5
6
7
4
6
8
10
12
14

Figure 4

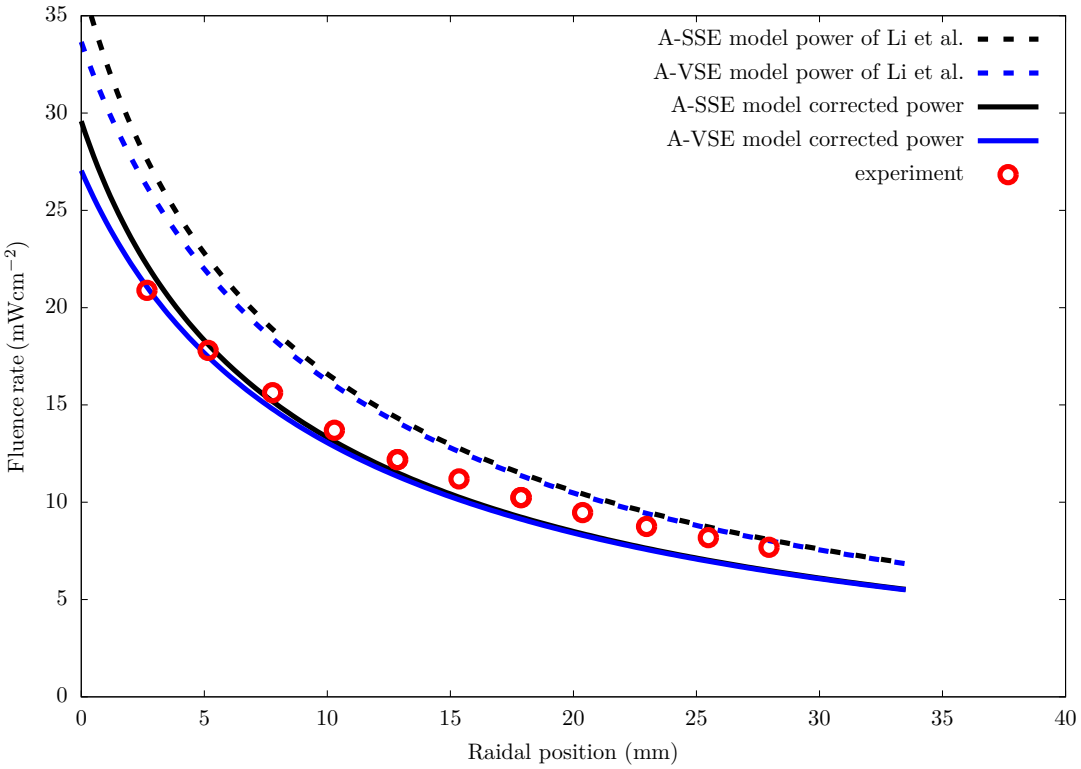
A-SSE model power of Li et al.
A-VSE model power of Li et al.
A-SSE model corrected power
A-VSE model corrected power
experiment
Fluence rate (mWcm^{-2})
Raidal position (mm)
0
5
10
15
20
25
30
35
40

Figure 5

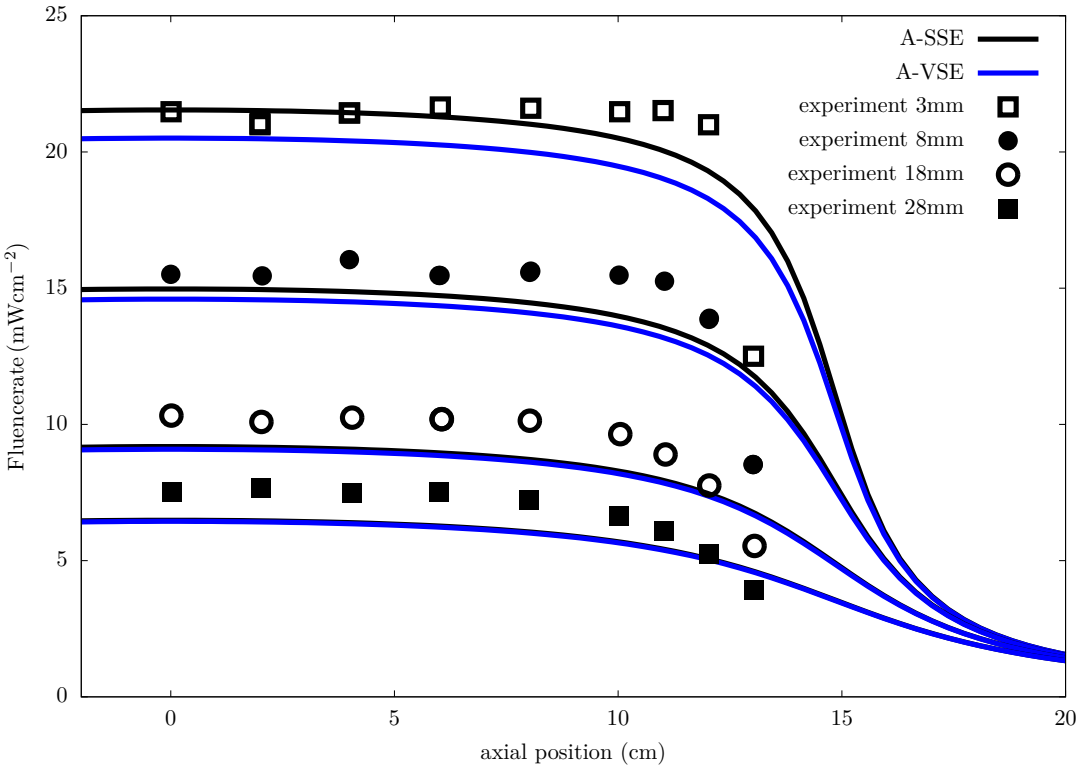
A-SSE
A-VSE
experiment 3mm
experiment 8mm
experiment 18mm
experiment 28mm
Fluencerate (mWcm^{-2})
axial position (cm)
0
5
10
15
20
25

Figure 6

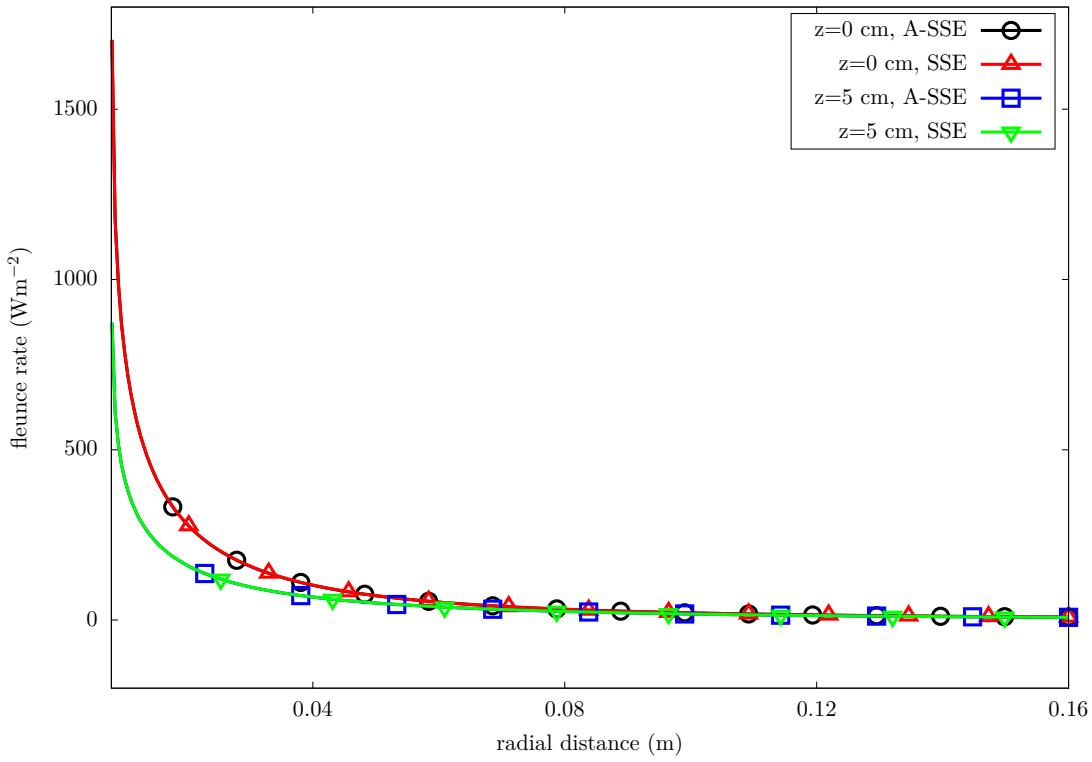
z=0 cm, A-SSE
z=0 cm, SSE
z=5 cm, A-SSE
z=5 cm, SSE
fleunce rate (Wm^{-2})
1500
1000
500
0
0.04
0.08
0.12
0.16
radial distance (m)

(a)

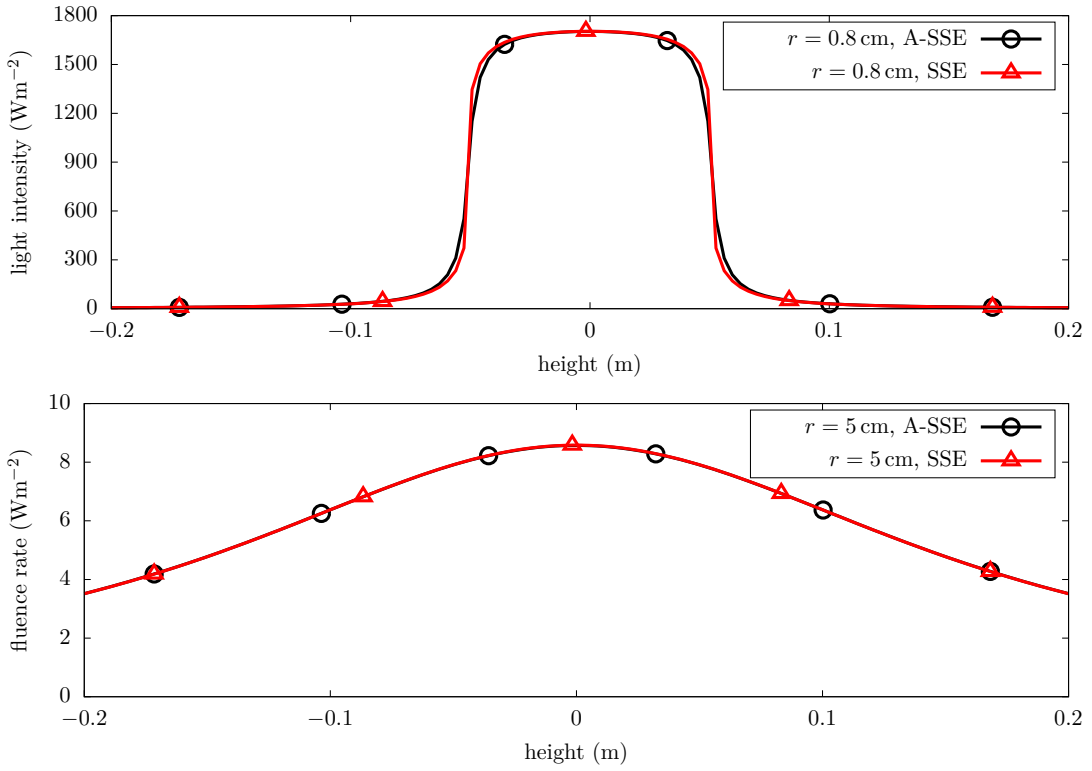
$r = 0.8$ cm, A-SSE
$r = 0.8$ cm, SSE
light intensity (Wm^{-2})
1800
1500
1200
900
600
300
0
−0.2
−0.1
0
0.1
0.2
height (m)
$r = 5$ cm, A-SSE
$r = 5$ cm, SSE
fluence rate (Wm^{-2})
10
8
6
4
2
0
−0.2
−0.1
0
0.1
0.2
height (m)

(b)

Figure 7

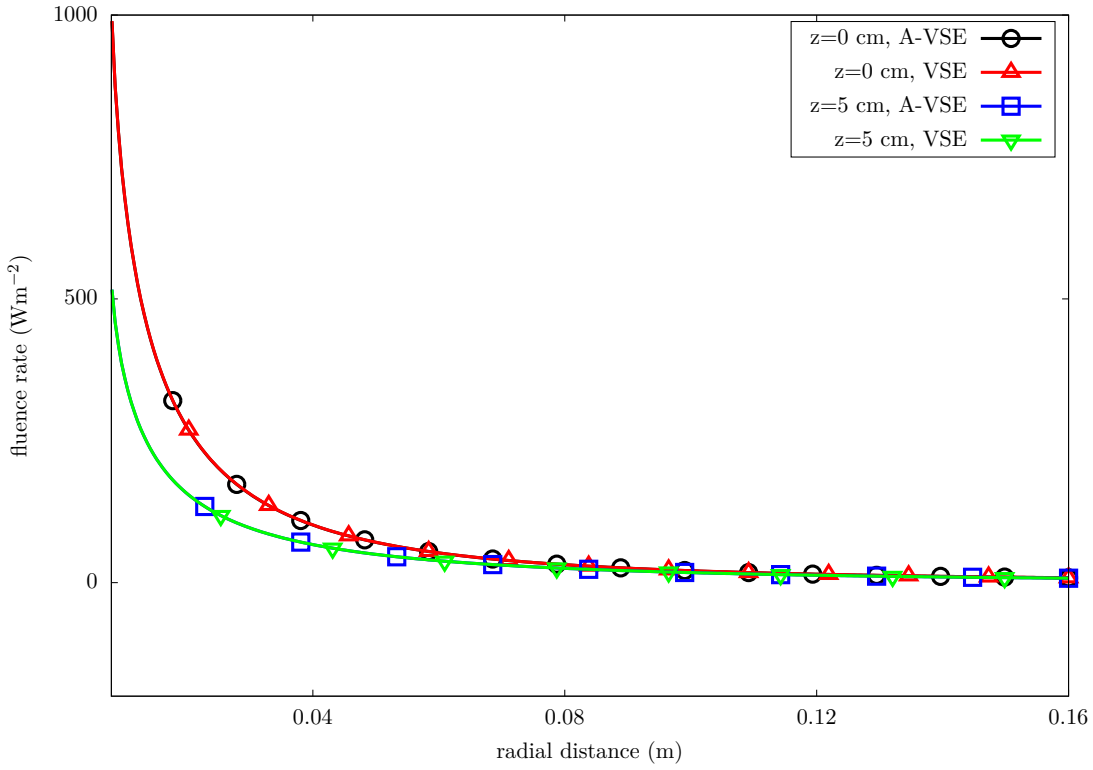
z=0 cm, A-VSE
z=0 cm, VSE
z=5 cm, A-VSE
z=5 cm, VSE
fluence rate (Wm^{-2})
radial distance (m)
1000
500
0
0.04
0.08
0.12
0.16

(a)

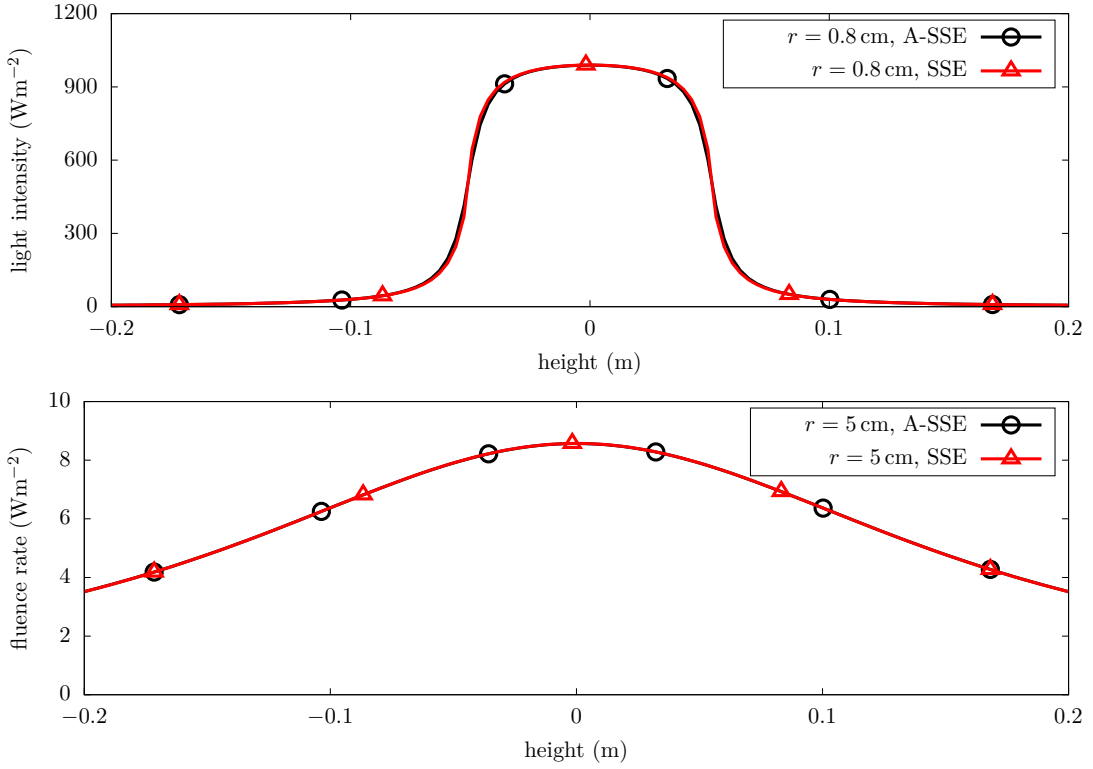
$r = 0.8$ cm, A-SSE
$r = 0.8$ cm, SSE
light intensity (Wm^{-2})
height (m)
1200
900
600
300
0
−0.2
−0.1
0
0.1
0.2
$r = 5$ cm, A-SSE
$r = 5$ cm, SSE
fluence rate (Wm^{-2})
height (m)
10
8
6
4
2
0
−0.2
−0.1
0
0.1
0.2

(b)

Figure 8